

Explicit formulation of second and third order optical nonlinearity in the FDTD framework

Charles Varin^{1,*}, Rhys Emms¹, Graeme Bart¹, Thomas Fennel², and Thomas Brabec¹

¹Center for Research in Photonics, University of Ottawa, Ottawa (ON) K1N 6N5, Canada

²Institut für Physik, Universität Rostock, 18051 Rostock, Germany

Abstract: The finite-difference time-domain (FDTD) method is a flexible and powerful technique for rigorously solving Maxwell's equations. However, three-dimensional optical nonlinearity in current commercial and research FDTD softwares requires solving iteratively an implicit form of Maxwell's equations over the entire numerical space and at each time step. Reaching numerical convergence demands significant computational resources and practical implementation often implies a complete rewriting of the core FDTD engine. In this paper, we present an explicit method to include second and third order optical nonlinearity in the FDTD framework based on a nonlinear generalization of the Lorentz dispersion model derived from an analytical solution of the quantum mechanical two-level equations. With the proposed approach, numerical integration is simple, intuitive, fully explicit, and computationally efficient.

References and links

1. A. Taflov and S. Hagness, *Computational Electrodynamics: The Finite-difference Time-domain Method* (Artech House, 2005).
2. A. Taflov, A. Oskooi, and S. Johnson, *Advances in FDTD Computational Electrodynamics: Photonics and Nanotechnology* (Artech House, 2013).
3. K. Yee, "Numerical solution of initial boundary value problems involving Maxwell's equations in isotropic media," *IEEE Trans. Antennas Propag.* **14**, 302–307 (1966).
4. J. P. Verboncoeur, "Particle simulation of plasmas: review and advances," *Plasma Phys. Control. Fusion* **47**, A231–A260 (2005).
5. C. Varin, C. Peltz, T. Brabec, and T. Fennel, "Attosecond plasma wave dynamics in laser-driven cluster nanoplasmas," *Phys. Rev. Lett.* **108**, 175007 (2012).
6. C. Peltz, C. Varin, T. Brabec, and T. Fennel, "Fully microscopic analysis of laser-driven finite plasmas using the example of clusters," *New J. Phys.* **14**, 065011 (2012).
7. C. Varin, C. Peltz, T. Brabec, and T. Fennel, "Light wave driven electron dynamics in clusters," *Ann. Phys.* **526**, 135–156 (2014).
8. C. Peltz, C. Varin, T. Brabec, and T. Fennel, "Time-resolved x-ray imaging of anisotropic nanoplasma expansion," *Phys. Rev. Lett.* **113**, 133401 (2014).
9. P. Goorjian, A. Taflov, R. Joseph, and S. Hagness, "Computational modeling of femtosecond optical solitons from Maxwell's equations," *IEEE J. Quantum Electron.* **28**, 2416–2422 (1992).
10. J. H. Greene and A. Taflov, "General vector auxiliary differential equation finite-difference time-domain method for nonlinear optics," *Opt. Express* **14**, 8305 (2006).
11. J. D. Jackson, *Classical Electrodynamics*, 3rd ed. (Wiley, 1998).
12. G. Fowles, *Introduction to Modern Optics*, Dover Books on Physics Series (Dover Publications, 1975).
13. R. Boyd, *Nonlinear Optics*, 3rd ed. (Elsevier Science, 2008).
14. D. Gordon, M. Helle, and J. Peñano, "Fully explicit nonlinear optics model in a particle-in-cell framework," *J. Comput. Phys.* **250**, 388–402 (2013).
15. M. Scalora, M. A. Vincenti, D. de Ceglia, C. M. Cojocaru, M. Grande, and J. W. Haus, "Nonlinear Duffing oscillator model for third harmonic generation," *J. Opt. Soc. Am. B* **32**, 2129 (2015).

16. M. Fejer, G. Magel, D. Jundt, and R. Byer, "Quasi-phase-matched second harmonic generation: tuning and tolerances," *IEEE J. Quantum Electron.* **28**, 2631–2654 (1992).
17. R. L. Byer, "Quasi-Phasematched Nonlinear Interactions and Devices," *J. Nonlinear Opt. Phys. Mater.* **06**, 549–592 (1997).
18. The C++ code we developed to solve this specific problem is available publicly at [\[location to be determined\]](#).
19. D. E. Zelmon, D. L. Small, and D. Jundt, "Infrared corrected Sellmeier coefficients for congruently grown lithium niobate and 5 mol.% magnesium oxide-doped lithium niobate," *J. Opt. Soc. Am. B* **14**, 3319–3322 (1997).
20. T. Lepetit and B. Kanté, "Nonlinear optics: Metamaterial quasi-phase matching," *Nature Photonics* **9**, 148–150 (2015).
21. N. Segal, S. Keren-Zur, N. Hendler, and T. Ellenbogen, "Controlling light with metamaterial-based nonlinear photonic crystals," *Nature Photonics* (2015).
22. G. P. Agrawal, *Nonlinear Fiber Optics*, 3rd ed. (Academic Press, San Diego, CA, 2001).
23. A. Couairon, E. Brambilla, T. Corti, D. Majus, O. de J. Ramírez-Góngora, and M. Kolesik, "Practitioners guide to laser pulse propagation models and simulation," *Eur. Phys. J. Spec. Top.* **199**, 5–76 (2011).
24. M. Kolesik and J. V. Moloney, "Modeling and simulation techniques in extreme nonlinear optics of gaseous and condensed media," *Reports on Progress in Physics* **77**, 016401 (2014).
25. T. D. Arber, K. Bennett, C. S. Brady, A. Lawrence-Douglas, M. G. Ramsay, N. J. Sircombe, P. Gillies, R. G. Evans, H. Schmitz, A. R. Bell, and C. P. Ridgers, "Contemporary particle-in-cell approach to laser-plasma modelling," *Plasma Phys. Control. Fusion* **57**, 113001 (2015).
26. I. H. Malitson, "Interspecimen Comparison of the Refractive Index of Fused Silica," *Journal of the Optical Society of America* **55**, 1205 (1965).
27. M. Fujii, M. Tahara, I. Sakagami, W. Freude, and P. Russer, "High-Order FDTD and Auxiliary Differential Equation Formulation of Optical Pulse Propagation in 2-D Kerr and Raman Nonlinear Dispersive Media," *IEEE J. Quantum Electron.* **40**, 175–182 (2004).
28. P. M. Goorjian and A. Taflove, "Direct time integration of Maxwells equations in nonlinear dispersive media for propagation and scattering of femtosecond electromagnetic solitons," *Opt. Lett.* **17**, 180 (1992).
29. L. Bergé, S. Skupin, R. Nuter, J. Kasparian, and J.-P. Wolf, "Ultrashort filaments of light in weakly ionized, optically transparent media," *Reports Prog. Phys.* **70**, 1633–1713 (2007).
30. A. Couairon and A. Mysyrowicz, "Femtosecond filamentation in transparent media," *Phys. Rep.* **441**, 47–189 (2007).
31. M. Kolesik, J. M. Brown, A. Teleki, P. Jakobsen, J. V. Moloney, and E. M. Wright, "Metastable electronic states and nonlinear response for high-intensity optical pulses," *Optica* **1**, 323 (2014).
32. C. Varin, G. Bart, R. Emms, and T. Brabec, "Saturable Lorentz model for fully explicit three-dimensional modeling of nonlinear optics," *Opt. Express* **23**, 2686–2695 (2015).
33. L. Allen and J. Eberly, *Optical Resonance and Two-level Atoms* (Dover, 1975).
34. A. Siegman, *Lasers* (University Science Books, 1986).

The finite-difference time-domain (FDTD) method is a powerful and flexible technique for the numerical integration of Maxwell's equations. It enables the rigorous study of optical, nanophotonic, and nanoplasmonic phenomena [1, 2]. It uses centered finite differences applied to all electric and magnetic components of the electromagnetic field to achieve second-order integration accuracy. The algorithm originally proposed in 1966 by Yee [3] solves the resulting set of coupled equations on three-dimensional numerical meshes, staggered in both space and time. Yee's approach remains today the most prominent numerical method for time-domain solutions of Maxwell's equations in complex settings. It is effectively used in commercial and research FDTD softwares [1, 2] and is a key component of the particle-in-cell [4] and microscopic particle-in-cell [5–8] techniques.

As surprising as it seems, the inclusion of optical nonlinearity in the Yee-FDTD framework is not straightforward. It is easily demonstrated with the Ampère's circuital law

$$\nabla \times \mathbf{H} - \epsilon_0 \frac{\partial \mathbf{E}}{\partial t} = \frac{\partial \mathbf{P}}{\partial t}, \quad (1)$$

where the source term would depend on a nonlinear susceptibility of the form $\mathbf{P} = \epsilon_0(\chi^{(1)}\mathbf{E} + \chi^{(2)}\mathbf{E}^2 + \chi^{(3)}\mathbf{E}^3 + \dots)$. This leads in Eq. (1) to a set of coupled nonlinear equations that are implicit in the electric field vector and whose solution is nontrivial [1, 9]. The current solving approach, proposed by Greene and Taflove [2, 10], uses a recursive Newton method to obtain an

approximate solution for \mathbf{E} . To ensure numerical convergence, it has to be performed over the entire numerical space at least a few times per time step, with a negative impact on computational performance. Despite its evident complexity for solving three-dimensional problems, the Greene-Taflove iterative method [10] is well established as a rigorous way to include optical nonlinearity into the FDTD framework [2].

In this paper, we develop an alternative approach for including optical nonlinearity in FDTD. The proposed method is based on a nonlinear generalization of the Lorentz oscillator equation, commonly used to model linear optical dispersion (see, e.g., [11]). Compared with the iterative Greene-Taflove technique, the advantages of the nonlinear Lorentz model are the following: (1) it is simple and intuitive, (2) numerical integration is fully explicit, and (3) it is flexible and computationally efficient. The proposed methodology is applied to the examples of second harmonic generation in a periodic structure and to the propagation of short optical pulses in dielectrics characterized by both the instantaneous (Kerr) and delayed (Raman) third-order nonlinearities.

This paper is divided as follows. First in Sec. 1, we present the nonlinear Lorentz model and its explicit integration in the Yee-FDTD framework. Next, in Sec. 2 we apply the nonlinear Lorentz model to the modelling of second harmonic generation (SHG) in periodically poled Lithium Niobate (PPLN). In Sec. 3, we present the nonlinear Lorentz model methodology to deal with short laser pulse propagation in centrosymmetric dielectrics and apply it to the particular case of optical solitons. In Sec. 4, we discuss a particular form of the nonlinear Lorentz model for strong field applications. We finally conclude in Sec. 5. Formal derivation of the nonlinear Lorentz model from the quantum mechanical two-level model equations is found in App. A.

1. The nonlinear Lorentz model

Optical dispersion is typically modeled with the following ordinary differential equation [11–13]

$$\frac{d^2 \mathbf{P}}{d\tau^2} + \frac{\gamma}{\omega_0} \frac{d\mathbf{P}}{d\tau} + \mathbf{P} = \epsilon_0 \tilde{\chi}^{(1)} \mathbf{E}, \quad (2)$$

also known as the Lorentz oscillator equation, where γ and ω_0 are respectively the collision and resonance frequencies, $\tau = \omega_0 t$ is the oscillator proper time, ϵ_0 is the vacuum permittivity, and $\tilde{\chi}^{(1)}$ is the *static* linear electric susceptibility. Eq. (2) is known to have the following solution in the Fourier-domain

$$\tilde{\mathbf{P}}(\omega) = \epsilon_0 \left(\frac{\omega_0^2}{\omega_0^2 - \omega^2 - i\gamma\omega} \right) \tilde{\chi}^{(1)} \tilde{\mathbf{E}}(\omega). \quad (3)$$

Going from Eq. (2) to Eq. (3), harmonic oscillation of the electric field \mathbf{E} and polarization density \mathbf{P} at the angular frequency ω was assumed to be as $e^{-i\omega t}$. Eq. (3) is used extensively to fit spectroscopic data, where multiple equations are combined to obtain satisfying dispersion curves over a certain spectral range, e.g.,

$$n^2(\omega) = 1 + \sum_k \left(\frac{\omega_k^2}{\omega_k^2 - \omega^2 - i\gamma_k\omega} \right) \tilde{\chi}_k^{(1)}, \quad (4)$$

where the subscript k refers to the parameters of the k th oscillator, with $\omega_k^2 \tilde{\chi}_k^{(1)}$ identified as the oscillator strength. In the particular case of dielectrics where conductivity can be neglected (i.e., all $\gamma_k \simeq 0$), Eq. (4) takes a particular form known as the Sellmeier formula (see, e.g., [12]).

The use of the oscillator proper time τ in Eq. (2) emphasizes the direct relationship between the static polarization density (i.e., \mathbf{P} in the limit where $d\mathbf{P}/d\tau \sim 0$) and the linear driving term on the right-hand side ($\epsilon_0 \tilde{\chi}^{(1)} \mathbf{E}$). Intuitively, nonlinear contributions to the polarization density are introduced by adding nonlinear source terms, e.g.,

$$\frac{d^2 \mathbf{P}}{d\tau^2} + \frac{\gamma}{\omega_0} \frac{d\mathbf{P}}{d\tau} + \mathbf{P} = \epsilon_0 \left(\tilde{\chi}^{(1)} \mathbf{E} + \tilde{\chi}^{(2)} \mathbf{E}^2 + \tilde{\chi}^{(3)} \mathbf{E}^3 + \dots \right). \quad (5)$$

A benefit of this formulation compared with, e.g., the anharmonic oscillator model [13–15], is a direct correspondence between the different numerical susceptibility parameters $\tilde{\chi}^{(n)}$ and those commonly used in perturbative nonlinear optics, generally obtained by measurements or *ab initio* calculations [13]. It is shown in App. A that Eq. (5) is in fact a valid form of the quantum mechanical two-level atom model in the under-resonant, adiabatic-following, weak-field limit.

In Eq. (5), the right-hand side contains the spectral information associated with the nonlinear conversion processes (harmonic generation), whereas the left-hand side defines how strongly the medium gets polarized by the different driving frequencies (dispersion). We stress that \mathbf{E} is the total electric field vector, i.e., $\mathbf{E} = \mathbf{E}_0 + \mathbf{E}_1 e^{-i\omega t} + \mathbf{E}_2 e^{-i2\omega t} + \dots$. It thus represents not only the incident signal oscillating at the dominant angular frequency ω_L of the laser spectrum, but also contributions coming from linear scattering ($\sim e^{-i\omega_L t}$) as well as nonlinear scattering and wave mixing ($\sim e^{-i0\omega_L t}, e^{-i\omega_L t}, e^{-i2\omega_L t}, e^{-i3\omega_L t}, \dots$).

For simplicity, in this paper the optical susceptibilities and oscillator parameters in Eq. (5) are represented by constants. However, a general formulation of the nonlinear Lorentz model must use tensors to account for the polarization dependent nature of light-matter interactions and allow proper modelling of the anisotropic optical response of a particular medium. Similarly to the Sellmeier's approach [see, e.g., Eq. (4)], multiple nonlinear Lorentz oscillators can be used to model specific linear and nonlinear dispersion curves, as demonstrated in Secs. 2 and 3.

1.1. Explicit numerical integration in the FDTD framework

We now demonstrate that integration of the nonlinear Lorentz model in the FDTD framework can be made fully explicit. Following the standard Yee procedure to express Maxwell's equations in terms of finite differences [1], one gets the following discretized equations for the electric and magnetic field vectors:

$$\mathbf{H}^{n+1/2} = \mathbf{H}^{n-1/2} - \frac{\Delta t}{\mu_0} (\nabla \times \mathbf{E})^n, \quad (6a)$$

$$\mathbf{E}^{n+1} = \mathbf{E}^n + \frac{\Delta t}{\epsilon_0} \left[(\nabla \times \mathbf{H})^{n+1/2} - \mathbf{J}^{n+1/2} \right], \quad (6b)$$

where n is the time index of the discretized time $t = n\Delta t$, with Δt being the numerical time step. We omitted the spatial indices voluntarily for simplicity (for details see, e.g., [1]). In this “free space fields” formulation, all material properties are contained in the current density $\mathbf{J}^{n+1/2}$.

Using $d\mathbf{P}/dt = \mathbf{J}$, Eq. (5) is written in terms of two first-order ordinary differential equations whose discretization is done to match Yee's staggering scheme. This results in the following leapfrog integration equations for the material polarization and current densities:

$$\mathbf{J}^{n+1/2} = \frac{(1-\Gamma)}{(1+\Gamma)} \mathbf{J}^{n-1/2} + \frac{\omega_0^2 \Delta t}{(1+\Gamma)} (\bar{\mathbf{P}}^n - \mathbf{P}^n) \quad (7a)$$

$$\mathbf{P}^{n+1} = \mathbf{P}^n + \Delta t \mathbf{J}^{n+1/2} \quad (7b)$$

where $\Gamma = \gamma\Delta t/2$ and $\bar{\mathbf{P}}^n = \epsilon_0 [\tilde{\chi}^{(1)} \mathbf{E}^n + \tilde{\chi}^{(2)} (\mathbf{E}^n)^2 + \tilde{\chi}^{(3)} (\mathbf{E}^n)^3 + \dots]$. It is seen immediately that in this form solving for $\mathbf{H}^{n+1/2}$ and \mathbf{E}^{n+1} , i.e., finding the electromagnetic field in the future,

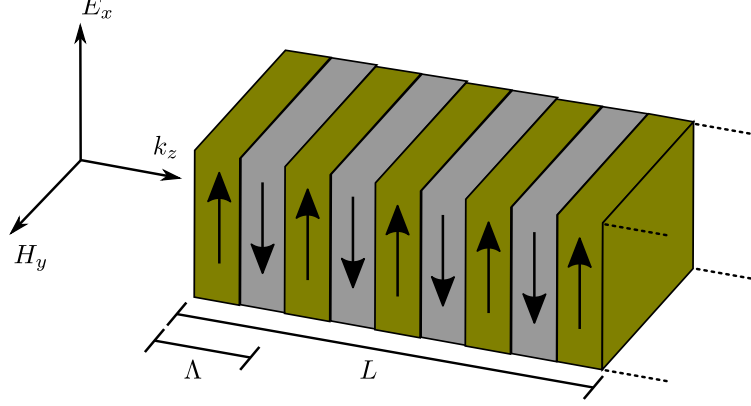


Fig. 1. Schematic representation of an electromagnetic plane wave impinging on an infinite PPLN crystal. Parameters L and Λ represent the distance away from the input face and the molecular orientation reversal period, respectively. The large-head black arrows indicate regions where the average permanent dipole moment is pointing up and down. With respect to the electric field E_x , this is associated with positive ($+\bar{\chi}_k^{(2)}$ for \uparrow) and negative ($-\bar{\chi}_k^{(2)}$ for \downarrow) second-order susceptibilities.

depends only on values in the past. Numerical integration of Eqs. (6a)-(7b) is thus fully explicit and does not require the Greene-Taflove iterative method [10].

In the next sections 2 and 3, we elaborate more on coupling the nonlinear Lorentz model to the FDTD technique by solving specific problems associated with light propagation in second and third order nonlinear media.

2. Example 1: second-harmonic generation in a periodically poled material

As a first example, we consider quasi-phase-matched second harmonic generation (QPM SHG) in a periodic structure, more specifically in periodically poled lithium niobate (PPLN) [13, 16, 17]. Technically, PPLN QPM SHG crystals are engineered by depositing metal electrodes directly on the crystal surface to which a strong voltage is applied to align the molecules and break the natural crystal symmetry [17]. By switching periodically the polarity of the strong voltage, it is possible to create a periodic array of domains with alternating positive and negative second order susceptibilities ($\pm\chi^{(2)}$). The reversal period is chosen to optimize the conversion efficiency of an input laser beam into its second harmonic. The modulation of the linear index is usually assumed to have a negligible impact [16]. Below, we show how FDTD modelling of QPM SHG can be performed with the help of the nonlinear Lorentz equation presented above.

For the demonstration, we considered a plane wave moving along the axis of an infinite PPLN crystal (see Fig. 1). For simplicity, we solved the corresponding 1D problem [18]. To include both the linear and nonlinear responses of the periodically poled domains, we used polarization equations like the following:

$$\frac{1}{\omega_k^2} \frac{d^2 P_k}{dt^2} + P_k = \epsilon_0 \left(\bar{\chi}_k^{(1)} E \pm \bar{\chi}_k^{(2)} E^2 \right), \quad (8)$$

where the sign of $\bar{\chi}_k^{(2)}$ is chosen to account for the direction of the local average molecular alignment and associated average permanent dipole moment (see again Fig. 1). The linear refractive index is assumed to be constant throughout the medium.

Effective modelling of optical dispersion in lithium niobate (LN) is achieved by using three oscillator equations like Eq. (8). We chose the linear part to match the Sellmeier formula for MgO doped LN (MgO:LN) [19]:

$$n^2(\omega) = 1 + \sum_{k=1}^3 \left(\frac{\omega_k^2}{\omega_k^2 - \omega^2} \right) \tilde{\chi}_k^{(1)}. \quad (9)$$

Values for the different parameters are given in Table 1. The nonlinear susceptibility was added to one of the equations according to typical values for commercial QPM crystals.

Table 1. Oscillator parameters used to model QPM SHG in periodically poled MgO:LN. Typical effective second order nonlinearity d_{eff} of commercial QPM crystals is in the 14 – 17 pm/V range, corresponding to $\tilde{\chi}^{(2)} \simeq 30$ pm/V. The nonlinearity can be added to only one of the three oscillator equations, usually to that with the largest resonance frequency (see [14] for details).

| k | $\tilde{\chi}_k^{(1)}$ | $\tilde{\chi}_k^{(2)}$ (pm/V) | ω_k (rad/s) |
|-----|------------------------|-------------------------------|-------------------------|
| 1 | 2.4272 | 30 | 1.5494×10^{16} |
| 2 | 1.4617 | 0 | 7.9514×10^{15} |
| 3 | 9.6536 | 0 | 9.7766×10^{13} |

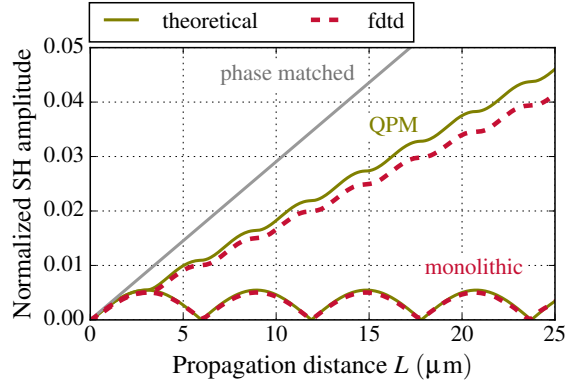


Fig. 2. Nonlinear-Lorentz/FDTD analysis of SHG in a QPM PPLN crystal. The amplitude of the second harmonic signal as a function of the distance L is compared with theory (Eqs. (2.2.12a) and (2.2.12b) in [13]). Laser pulse parameters were: intensity 5×10^8 W/cm², duration 10 fs, and central wavelength $\lambda_0 = 1.064 \mu\text{m}$.

In Fig. 2, we compared the nonlinear-Lorentz/FDTD analysis to a conventional theoretical model for QPM SHG [13, 16, 17]. Theoretical curves were obtained by integrating numerically Eqs. (2.2.12a) and (2.2.12b) in [13]. For the FDTD curves, we performed simulations of a 40- μm -thick medium slab in a 80- μm domain (ended by absorbing boundaries) discretized with a 4-nm resolution. A Gaussian laser pulse was initially outside the numerical domain and propagated through it for 0.8 ps with $\Delta t \simeq 13$ as. We sampled the electric field at 500 positions regularly spaced in the medium and took the absolute value of the Fourier transform of each of the 500 time traces ($E(t)$) to find the spectral amplitude of the second harmonic ($|E(2\omega_L)|$). These SH amplitudes were ultimately normalized by the amplitude of the incident electric field ($E_0 = \sqrt{2\eta_0 I}$, with I being the laser intensity) and mapped to the corresponding position in the medium. Results are shown in Fig. 2.

For a medium without a periodic structure (monolithic), the amplitude of the second-harmonic signal ($2\omega_L$) oscillates due to the wave vector mismatch with respect to the input signal (ω_L). The oscillation period Λ depends effectively on the mismatch parameter $\Delta k = (2\omega_L/c)[n(\omega_L) - n(2\omega_L)]$, while the amplitude of the oscillation is proportional to $\bar{\chi}^{(2)}I$ [13]. The excellent agreement between theory and FDTD in Fig. 2 demonstrates that the nonlinear-Lorentz/FDTD analysis succeeds at reproducing quantitatively the dispersion, scattering, and wave mixing processes in SHG, as well as their interplay.

Quasi phase matching (QPM) consists in bypassing the wave vector mismatch by inverting the sign of $\chi^{(2)}$ periodically to make the SH signal grow continuously. With the parameters presented in Table 1, the optimal sign reversal period is $\Lambda_{\text{QPM,opt}} = 2\pi/\Delta k \simeq 5.9 \mu\text{m}$. Periodic poling was implemented in both the theoretical model and FDTD by setting the sign of $\bar{\chi}^{(2)}$ with the spatial function $\text{sign}[\sin(2\pi z/\Lambda_{\text{QPM,opt}})]$, with $z = 0$ corresponding to the input face of the crystal.

Results for QPM SHG in Fig. 2 show a significant difference between theory and nonlinear-Lorentz/FDTD. Although both curves are qualitatively the same, the SH average growth rate is lower for FDTD. We emphasize that the theoretical curves in Fig. 2 were corrected to account for *linear* reflection at the input face of the crystal via the intensity transmission coefficient $T_I = 4/(1 + n(\omega_L))^2$, where $n(\omega)$ is the linear refractive index given by Eq. (9). But spectral analysis of the FDTD results revealed a non-negligible reflection at $2\omega_L$ and around $0\omega_L$. In fact, we observed that if we reduce the transmission coefficient by only 9%, i.e., with $T'_I = 0.91T_I$, theory and FDTD curves lie perfectly on each other. This suggests that *nonlinear* reflection at the crystal input face, that is not accounted for by the theoretical model, has a non-negligible influence in this particular problem.

Summing up, in this section we have shown that quantitative insight into subwavelength nonlinear scattering and wave-mixing processes is possible with the nonlinear-Lorentz/FDTD approach. A three-dimensional generalization of the one-dimensional analysis we have provided is straightforward. Finite transverse beam profile and medium response anisotropy (birefringence) are easy to include as well. The flexibility and reliability of the nonlinear-Lorentz/FDTD method offer an exceptional potential for modelling SHG and other nonlinear phenomena in complex settings, e.g., for the analysis of SHG in metamaterial devices [20, 21].

3. Example 2: short pulse propagation in centrosymmetric dielectrics

In centrosymmetric dielectrics, the optical Kerr effect is responsible for third-harmonic generation and the intensity-dependent modification of the refractive index. For laser pulses with a finite duration, an accurate description of these processes must include both the nearly-instantaneous electronic response (instantaneous Kerr) and a delayed component associated with stimulated molecular Raman scattering (Raman) [13]. This is suitably represented by the following equation for the third-order polarization density [22]:

$$\mathbf{P}^{(3)}(t) = \epsilon_0 \chi^{(3)} \mathbf{E} \int_{-\infty}^t g(t-t') |\mathbf{E}(t')|^2 dt', \quad (10)$$

where $g(t) = \alpha\delta(t) + (1 - \alpha)h_R(t)$. Good approximate forms for the instantaneous Kerr and Raman response functions are, respectively, a Dirac delta function $\delta(t)$ and

$$h_R(t) = \left(\frac{\tau_1^2 + \tau_2^2}{\tau_1 \tau_2} \right) e^{-t/\tau_2} \sin(t/\tau_1), \quad (11)$$

with parameters τ_1 and τ_2 chosen to fit the Raman-gain spectrum [22]. The balance between the instantaneous and delayed contributions is parametrized by α .

For numerical integration, it is convenient to avoid the convolution in Eq. (10) by defining a generalized rotation/vibration coordinate Q whose time evolution is given by the following differential equation [10, 23, 24]:

$$\frac{d^2 Q}{dt^2} + 2\gamma_R \frac{dQ}{dt} + \omega_R^2 Q = \omega_R^2 |\mathbf{E}|^2, \quad (12)$$

where $\omega_R = \sqrt{(\tau_1^2 + \tau_2^2)/\tau_1^2 \tau_2^2}$ and $\gamma_R = 1/\tau_2$. The third-order polarization density is then:

$$\mathbf{P}^{(3)}(t) = \underbrace{\varepsilon_0 \tilde{\chi}^{(3)} \alpha \mathbf{E}^3}_{\text{instantaneous Kerr}} + \underbrace{\varepsilon_0 \tilde{\chi}^{(3)} (1 - \alpha) Q \mathbf{E}}_{\text{Raman}}. \quad (13)$$

For integration of Eqs. (12) and (13) in FDTD, Greene and Taflovie [2, 10] proposed to define a current density from two consecutive polarization densities, e.g.,

$$\mathbf{J}_{Raman}^{n+1/2} \propto \frac{Q^{n+1} \mathbf{E}^{n+1} - Q^n \mathbf{E}^n}{\Delta t}, \quad (14)$$

which leads to implicit FDTD equations that need to be solved iteratively to obtain an approximate solution for \mathbf{E}^{n+1} [2, 10]. Instead, explicit FDTD integration with third-order nonlinearity can be done with the following nonlinear Lorentz equation:

$$\frac{d^2 \mathbf{P}}{d\tau^2} + \frac{\gamma}{\omega_0} \frac{d\mathbf{P}}{d\tau} + \mathbf{P} = \varepsilon_0 \tilde{\chi}^{(1)} \mathbf{E} + \varepsilon_0 \tilde{\chi}^{(3)} [\alpha \mathbf{E}^3 + (1 - \alpha) Q \mathbf{E}]. \quad (15)$$

Discretization of Eqs. (12) and (15) leads to the fully explicit update sequence that follows:

1. Evaluate $\bar{\mathbf{P}}^n = \varepsilon_0 \tilde{\chi}^{(1)} \mathbf{E}^n + \varepsilon_0 \tilde{\chi}^{(3)} [\alpha (\mathbf{E}^n)^3 + (1 - \alpha) Q^n \mathbf{E}^n]$.
2. Update the current and polarization densities with Eqs. (7a) and (7b).
3. Update Q with

$$G^{n+1/2} = \frac{(1 - \Gamma_R)}{(1 + \Gamma_R)} G^{n-1/2} + \frac{\omega_R^2 \Delta t}{(1 + \Gamma_R)} [(\mathbf{E}^n)^2 - Q^n] \quad (16a)$$

$$Q^{n+1} = Q^n + \Delta t G^{n+1/2}, \quad (16b)$$

where $\Gamma_R = \Delta t \gamma_R$.

4. Update the electromagnetic field with Eqs. (6a) and (6b).

For demonstration, we implemented this update sequence in the particle-in-cell code EPOCH [25]. As a practical example, we considered the 1D propagation of a short optical pulse in fused silica and used EPOCH's moving window feature to track the pulse (the window moves with the pulse at the group velocity). Medium parameters are summarized in Table 2 (see table caption for other definitions used below).

We recall that the propagation of intense and short light pulses in dielectrics is directly influenced by both the linear and nonlinear responses of the medium. We have shown in the previous section that these effects are correctly accounted for by the nonlinear Lorentz model. In 1D and in the presence of anomalous dispersion ($\beta_2 < 0$), the interplay between group velocity dispersion (GVD) and self-phase modulation (SPM) can manifest itself in a spectacular way by the formation of temporal optical solitons [22]. In the case of a fundamental soliton ($N^2 = L_D/L_{NL} \sim 1$), GVD and SPM are perfectly balanced and the pulse shape and spectrum

Table 2. Parameters used to model optical pulse propagation in fused silica [22, 26]. The third order susceptibility parameter $\tilde{\chi}_k^{(3)}$ was obtained from the third order nonlinear index $n_2 = 2.59 \times 10^{-20} \text{ m}^2/\text{W}$ measured at a reference wavelength of $1.5 \mu\text{m}$ [22]. The corresponding nonlinear length is $L_{\text{NL}} = (n_2 I \omega_0 / c)^{-1} \simeq 9.22 \times 10^{12} \text{ m}/I$, where I is the laser intensity expressed in W/m^2 . The group velocity dispersion (GVD) parameter $\beta_2 \simeq -22.2 \text{ fs}^2/\text{mm}$ is readily obtained from the Sellmeier equation, which allows to define the dispersion length $L_D = T^2/|\beta_2| \simeq 45 \mu\text{m} \times (T[\text{fs}])^2$, where $T[\text{fs}]$ is the pulse duration in femtosecond.

| k | $\tilde{\chi}_k^{(1)}$ | $\omega_k \text{ (rad/s)}$ | $\tilde{\chi}_k^{(3)} \text{ (m}^2/\text{V}^2\text{)}$ | α | $\omega_R \text{ (rad/s)}$ | $\gamma_R \text{ (1/s)}$ |
|-----|------------------------|----------------------------|--|----------|----------------------------|--------------------------|
| 1 | 0.69617 | 2.7537×10^{16} | 1.94×10^{-22} | 0.7 | 8.7722×10^{13} | 3.1250×10^{13} |
| 2 | 0.40794 | 1.6205×10^{16} | 0 | 0 | 0 | 0 |
| 3 | 0.89748 | 1.9034×10^{14} | 0 | 0 | 0 | 0 |

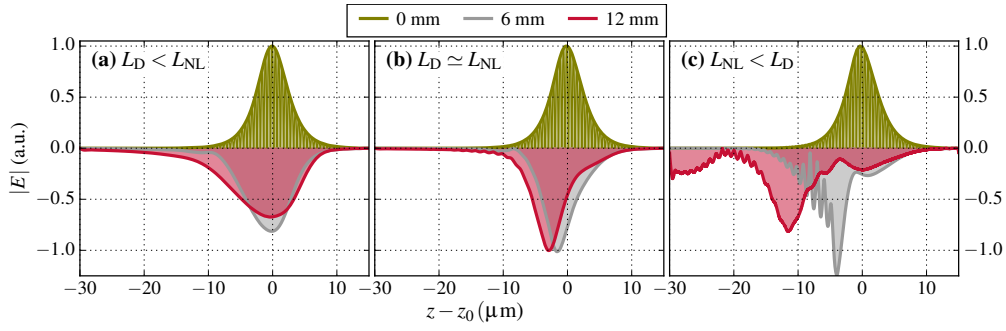


Fig. 3. Nonlinear-Lorentz/FDTD analysis of soliton propagation in fused silica. Color-coded are the pulse envelopes obtained by taking the absolute value of the Hilbert transform of the pulse snapshots at different propagation distances z_0 (see legend). In (a) where $I = 10^8 \text{ W}/\text{cm}^2$, group velocity dispersion dominates and the initial pulse $[\propto \text{sech}(t/t_0)]$, with $t_0 = 10 \text{ fs}$ spreads as it propagates. In (b) where $I = 3.25 \times 10^{11} \text{ W}/\text{cm}^2$, the pulse propagates with nearly-constant width and amplitude over a distance greater than the soliton period $\pi L_D/2 \simeq 7 \text{ mm}$, suggesting that it is effectively a fundamental soliton [22]. The shift of the peak toward the left $[(z - z_0) < 0]$ indicates that this soliton propagates at a slower group velocity than in (a). In (c) where $I = 10^{12} \text{ W}/\text{cm}^2$, nonlinearity dominates and the pulse self-focuses temporally before breaking up due to modulation instability. We stress that the origin of the z axis, i.e., $z = z_0$, corresponds to a reference point moving at the linear group velocity.

remain constant during propagation. This particular optical effect was used by several authors to test nonlinear models in FDTD [10, 27, 28]. For a 10-fs pulse at a $1.5 \mu\text{m}$ wavelength in fused silica, the fundamental soliton condition is fulfilled when the laser intensity is on the order of $10^{11} \text{ W}/\text{cm}^2$. Results shown in Fig. 3 are in good agreement with this prediction and similar tests found in [10, 27, 28]. This demonstrates, again, the capability of the nonlinear-Lorentz/FDTD approach to model quantitatively linear and nonlinear optical processes and their interplay.

We emphasize that in previous works [10, 27, 28], simulations were done with scaled parameters to ensure that optical solitons were observable within short propagation distances ($< 200 \mu\text{m}$) with reasonable computational resources. In particular in [27], authors used $\chi^{(3)} = 7 \times 10^{-2} \text{ m}^2/\text{V}^2$ with a $1 \text{ V}/\text{m}$ pulse peak electric field amplitude. With physically relevant material parameters like in the current work, this is equivalent to a laser intensity of

$\sim 4.8 \times 10^{13} \text{ W/cm}^2$, which is typically the light intensity inside a laser filament [29, 30]. In this extreme regime the nonlinear material response is non-perturbative and accurate modelling of light-matter interaction must take material ionization and breakdown into account. Proper coverage of this complex topic is far beyond the scope of this paper. Nevertheless, in the next section we propose a particular form of the nonlinear Lorentz model suitable for strong-field applications, assuming that it would be complemented with proper models for the ionization and plasma dynamics.

4. The strong-field nonlinear Lorentz model

The specific form of the nonlinear Lorentz oscillator equation shown in Eq. (5) is not unique. For example, the anharmonic oscillator equation shares similar properties [13–15]. In fact, in the under-resonant ($\omega \ll \omega_0$) weak-field limit ($\tilde{\chi}^{(3)}|\mathbf{E}|^2 \ll \tilde{\chi}^{(1)}$), both Eq. (5) and the anharmonic oscillator converge trivially to the Lorentz dispersion model of Eq. (3). However, in the strong-field limit their respective behavior is significantly different.

A rigorous treatment of strong-field optical phenomena requires quantum mechanics (see, e.g., [31]). Nevertheless, in a previous work [32] we have shown that the driving force of an oscillator can be chosen in a way to reproduce the polarization obtained from the solution of the quantum mechanical two-level equations in the under-resonant limit. In terms of the formalism developed in this paper, the strong-field oscillator of [32] reads

$$\frac{d^2\mathbf{P}}{d\tau^2} + \frac{\gamma}{\omega_0} \frac{d\mathbf{P}}{d\tau} + \mathbf{P} = \epsilon_0 \tilde{\chi}^{(1)} \left(\frac{1}{1 + \tilde{\chi}^{(3)}|\mathbf{E}|^2/\tilde{\chi}^{(1)}} \right) \mathbf{E}. \quad (17)$$

In the weak-field limit, it expands to

$$\frac{d^2\mathbf{P}}{d\tau^2} + \frac{\gamma}{\omega_0} \frac{d\mathbf{P}}{d\tau} + \mathbf{P} = \epsilon_0 \left(\tilde{\chi}^{(1)} - \tilde{\chi}^{(3)}|\mathbf{E}|^2 + \dots \right) \mathbf{E}. \quad (18)$$

Comparing Eq. (18) with Eq. (5), it appears that Eq. (17) effectively models the polarizability of a centrosymmetric material ($\tilde{\chi}^{(2)} = 0$) with a *negative* instantaneous Kerr nonlinearity. Most media are effectively characterized by a *positive* Kerr index (see, e.g., [13]). When compared with Eq. (26), it appears that an appropriate form of the strong-field oscillator equation for a *positive* Kerr response is instead:

$$\frac{d^2\mathbf{P}}{d\tau^2} + \frac{\gamma}{\omega_0} \frac{d\mathbf{P}}{d\tau} + \mathbf{P} = \epsilon_0 \tilde{\chi}^{(1)} \left(2 - \frac{1}{1 + \tilde{\chi}^{(3)}|\mathbf{E}|^2/\tilde{\chi}^{(1)}} \right) \mathbf{E}, \quad (19)$$

with the following weak-field limit:

$$\frac{d^2\mathbf{P}}{d\tau^2} + \frac{\gamma}{\omega_0} \frac{d\mathbf{P}}{d\tau} + \mathbf{P} = \epsilon_0 \left(\tilde{\chi}^{(1)} + \tilde{\chi}^{(3)}|\mathbf{E}|^2 - \dots \right) \mathbf{E}. \quad (20)$$

Although Eqs. (17) and (19) are characterized by identical linear and nonlinear polarization spectral amplitudes $|\tilde{\mathbf{P}}(\omega)|$, they differ by the relative phase between the linear and the third harmonic signals. This difference is such that a laser beam propagating in a medium modelled with Eqs. (17) or (18) will experience self-defocusing ($-\tilde{\chi}^{(3)}$), whereas in a medium modelled with Eqs. (19) or (20) it will experience self-focusing ($\tilde{\chi}^{(3)}$).

We summarized in Table 3 different oscillator equations that can be used to integrate the instantaneous optical Kerr nonlinearity explicitly in FDTD via Eqs. (7a) and (7b). We compared their numerical behavior against the quantum mechanical two-level model given by Eqs. (6.5.6) and (6.5.8) in [13]. The results in Fig. 4 clearly show that in the strong-field limit only the

Table 3. Comparison between different nonlinear harmonic oscillator models that follow an equation like $\frac{d^2\mathbf{P}}{d\tau^2} + \frac{\gamma}{\omega_0} \frac{d\mathbf{P}}{d\tau} + \mathbf{P} = \bar{\mathbf{P}}$, where $\bar{\mathbf{P}}$ is a static polarization density that contains the nonlinearity and $\tau = \omega_0 t$ is the oscillator proper time. The parameter b below is the anharmonic constant, proportional to an effective $\chi^{(3)}$ (see [13–15], and also App. A). All these oscillator models can be integrated explicitly in FDTD via Eqs. (7a) and (7b), with the appropriate form for $\bar{\mathbf{P}}$.

| Name | $\bar{\mathbf{P}}$ | Refs. |
|-------------------|---|-------------------|
| Lorentz | $\epsilon_0 \bar{\chi}^{(1)} \mathbf{E}$ | [12] |
| Nonlinear Lorentz | $\epsilon_0 \left(\bar{\chi}^{(1)} + \bar{\chi}^{(3)} \mathbf{E} ^2 \right) \mathbf{E}$ | Eq. (5) |
| Anharmonic | $\epsilon_0 \bar{\chi}^{(1)} \mathbf{E} + b \mathbf{P}^3$ | [13–15], Eq. (29) |
| Strong-field | see Eqs. (17) and (19) | see also [32] |

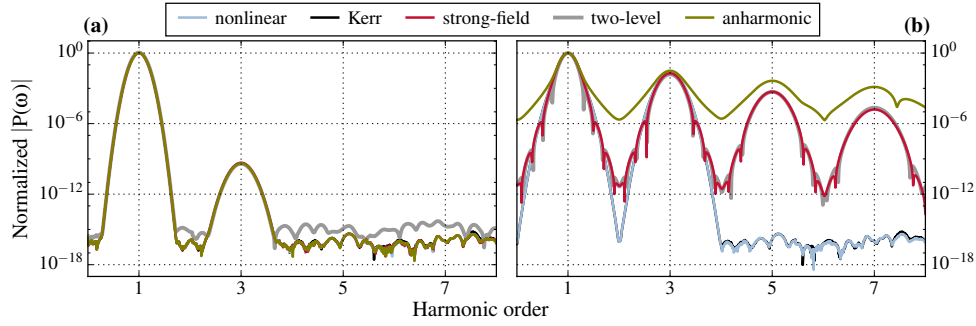


Fig. 4. Comparison between the nonlinear oscillator models summarized in Table 3. While in (a) their weak-field ($I = 10^6 \text{ W/cm}^2$) solutions match perfectly, in (b) their strong-field behaviors ($I = 5 \times 10^{13} \text{ W/cm}^2$) differ significantly. In (b), the strong-field Lorentz model characterized by Eqs. (17) and (19) can effectively reproduce the polarization of the quantum mechanical two-level model (see Eqs. (6.5.6) and (6.5.8) in [13]), whereas the nonlinear Lorentz model [see Eq. (5)] follows the instantaneous Kerr polarization $P = \epsilon_0 \left(\bar{\chi}^{(1)} E + \bar{\chi}^{(3)} E^3 \right)$. For strong fields, the integration of the anharmonic oscillator is unstable and fails at reproducing any of the two-level or instantaneous Kerr polarizations. For these tests, we used fictitious values for the oscillator parameters ($\gamma = 0$ and $\omega_0 = 3 \times 10^{16} \text{ rad/s}$) and susceptibilities ($\bar{\chi}^{(1)} = 5 \times 10^{-4}$ and $\bar{\chi}^{(3)} = 1.6 \times 10^{-25} \text{ m}^2/\text{V}^2$) similar to those for air at ambient pressure. The two-level model and the anharmonic b parameters were set so that all results agree in the weak-field limit shown in (a). The driving electric field was that of a 10-fs Gaussian pulse with $\lambda_0 = 800 \text{ nm}$.

strong-field Lorentz model characterized by Eqs. (17) and (19) can effectively reproduce the response associated with the quantum mechanical two-level equation, whereas the nonlinear Lorentz model follows an instantaneous Kerr polarization of the form $P = \epsilon_0 \left(\bar{\chi}^{(1)} E + \bar{\chi}^{(3)} E^3 \right)$. In the strong-field regime, the anharmonic oscillator solution fails at reproducing any of the two-level or instantaneous Kerr polarizations.

Finally, it is straightforward to show that a strong-field formulation of the nonlinear Lorentz model that includes the Raman contribution can be written as :

$$\frac{d^2\mathbf{P}}{d\tau^2} + \frac{\gamma}{\omega_0} \frac{d\mathbf{P}}{d\tau} + \mathbf{P} = \epsilon_0 (1 - \alpha) \bar{\chi}^{(3)} \mathcal{Q} \mathbf{E} + \epsilon_0 \bar{\chi}^{(1)} \left(2 - \frac{1}{1 + \alpha \bar{\chi}^{(3)} |\mathbf{E}|^2 / \bar{\chi}^{(1)}} \right) \mathbf{E}, \quad (21)$$

where Q is determined by Eq. (12). Explicit integration of Eq. (21) in FDTD is done as presented in Sec. 3.

5. Conclusions

In this paper, we have presented an extension of the Lorentz dispersion model to include nonlinear optics in the FDTD framework. Compared with the current iterative techniques, its numerical integration is simple, intuitive, fully explicit, computationally efficient, and flexible. A complete methodology was elaborated, supported by full-scale FDTD tests that were compared with known and accepted theoretical models and calculations. Three-dimensional FDTD implementation is straightforward due to the inherent vectorial nature of the model, with the possibility to include damping, restoring, and light-matter coupling in a tensorial form to allow effective modeling of anisotropic nonlinear response. Finally, we proposed and analyzed a formulation of the nonlinear Lorentz model suitable for strong field applications. In particular, we have shown that it should be used in replacement of the anharmonic (Duffing) oscillator that tends to be unstable and inaccurate for intense fields. Ultimately, the use of the strong-field nonlinear Lorentz model in FDTD-based plasma simulation approaches like PIC and MicPIC promises insight into the light-matter interaction processes involved in situations where both the dielectric polarization and plasma dynamics are important, e.g., during laser filamentation and femtosecond micromachining of dielectrics.

A. Quantum foundations : the two-level atom revisited

The quantum mechanical two-level atom model provides a good approximation to a more complete theory of nonlinear optics [13, 33]. Its harmonic oscillator formulation is characterized by the following coupled equations [13, 34]:

$$\frac{d^2 \mathbf{p}}{dt^2} + \frac{2}{T_2} \frac{d\mathbf{p}}{dt} + \omega_0^2 \mathbf{p} = -\kappa w \mathbf{E} \quad (22)$$

$$\frac{dw}{dt} + \frac{w - w^{eq}}{T_1} = \left(\frac{2}{\hbar \omega_0} \right) \mathbf{E} \cdot \frac{d\mathbf{p}}{dt}. \quad (23)$$

\mathbf{E} is the electric field vector of the driving signal, \mathbf{p} is the expectation value of the induced dipole moment, w is the population inversion parameter with equilibrium value w^{eq} , $\kappa = 2\omega_0 d_0^2 / \hbar$ is an atom-field coupling parameter, d_0 is the atomic dipole moment constant, $\hbar \omega_0$ is the transition energy between the two levels, T_1 is the population relaxation time, and T_2 is the atomic dephasing time.

In the linear limit where $w \simeq -1$, Eqs. (22) and (23) simplify to the Lorentz dispersion model given at Eq. (2). Below, we look at the perturbative nonlinear regime to find an approximate solution for the population parameter $w(t)$. When this approximate solution is reintroduced in Eq. (22) and Taylor expanded in powers of $|\mathbf{E}|^2$ around $|\mathbf{E}|^2 = 0$, the nonlinear Lorentz model equation [Eq. (5)] is found.

We first consider an electromagnetic pulse whose electric field is defined by $\mathbf{E}(t) = \mathbf{E}_0 \sin(\omega t) \exp(-t^2/t_p^2)$, with amplitude \mathbf{E}_0 , angular frequency ω , and duration t_p . Then, we assume that the atom-light interaction is under-resonant ($\omega \ll \omega_0$). Next, we consider the adiabatic-following approximation by assuming that the duration of the pulse is short enough so that we can neglect the two relaxation constants ($t_p \ll T_1, T_2$) by taking $T_2 \rightarrow \infty$ and $T_1 \rightarrow \infty$ in Eqs. (22) and (23), respectively. Under these approximations, $\mathbf{p} \simeq -\kappa w \mathbf{E} / \omega_0^2$ and

$$\frac{dw}{dt} \simeq - \left(\frac{2\kappa}{\hbar \omega_0^3} \right) \left[|\mathbf{E}|^2 \frac{dw}{dt} + \frac{w}{2} \frac{d|\mathbf{E}|^2}{dt} \right], \quad (24)$$

where $|\mathbf{E}|^2 = \mathbf{E} \cdot \mathbf{E}$ is a quantity oscillating at twice the laser frequency ω , in comparison with the envelope (associated with $\mathbf{E} \cdot \mathbf{E}^*$). Eq. (24) has the exact solution that follows:

$$w = \frac{1}{\sqrt{1 + \left(\frac{2\kappa}{\hbar\omega_0^3}\right) |\mathbf{E}|^2}} + C, \quad (25)$$

in agreement with [13]. In the limit $t \rightarrow -\infty$, $\mathbf{E} = 0$ and $w = -1$ (the population is in the ground state), leading to $C = -2$. Replacing w in Eq. (22) by Eq. (25) then gives:

$$\frac{d^2 p}{dt^2} + \frac{2}{T_2} \frac{dp}{dt} + \omega_0^2 p = \kappa \left(2 - \frac{1}{\sqrt{1 + \left(\frac{2\kappa}{\hbar\omega_0^3}\right) |\mathbf{E}|^2}} \right) \mathbf{E}, \quad (26)$$

which is a quantum mechanically valid form of the two-level atom model in the under-resonant, adiabatic-following limit. The validity conditions of this equation are typically met for moderately intense femtosecond pulses in dielectrics. Expanding the square root in powers of $(2\kappa/\hbar\omega_0^3) |\mathbf{E}|^2$ further gives:

$$\frac{d^2 p}{dt^2} + \frac{2}{T_2} \frac{dp}{dt} + \omega_0^2 p = \kappa \mathbf{E} + \frac{\kappa}{2} \left(\frac{2\kappa}{\hbar\omega_0^3} \right) \mathbf{E}^3 - \frac{3\kappa}{8} \left(\frac{2\kappa}{\hbar\omega_0^3} \right)^2 \mathbf{E}^5 + \dots, \quad (27)$$

Eq. (5) is evidently a legitimate generalization of Eq. (27) for both centrosymmetric and non-centrosymmetric media.

It is interesting to develop further Eq. (27) by inserting the linearized ($w \simeq -1$) under-resonant adiabatic-following relationship $\mathbf{p} \simeq -\kappa w \mathbf{E} / \omega_0^2 \simeq \kappa \mathbf{E} / \omega_0^2$ into the nonlinear source terms such that:

$$\frac{d^2 \mathbf{p}}{dt^2} + \frac{2}{T_2} \frac{d\mathbf{p}}{dt} + \omega_0^2 \mathbf{p} = \kappa \mathbf{E} + \frac{\kappa}{2} \left(\frac{2\kappa}{\hbar\omega_0^3} \right) \left(\frac{\omega_0^2}{\kappa} \right)^3 \mathbf{p}^3 - \mathcal{O}(\mathbf{p}^5) + \dots \quad (28)$$

After simplifying and rearranging terms:

$$\frac{d^2 \mathbf{p}}{dt^2} + \frac{2}{T_2} \frac{d\mathbf{p}}{dt} + \omega_0^2 \mathbf{p} - \frac{1}{2} \left(\frac{\omega_0}{d_0} \right)^2 \mathbf{p}^3 + \mathcal{O}(\mathbf{p}^5) - \dots = \kappa \mathbf{E}. \quad (29)$$

Eq. (29) is identified as the anharmonic (Duffing) oscillator equation with a nonlinear parameter $b = \omega_0^2 / 2d_0^2$ (see, e.g., [14, 15]). From the derivation we provided, it appears that it is also a quantum mechanically valid form of the two-level atom model equations in the under-resonant, adiabatic-following, weak-field limit. However, the use of $w \simeq -1$ implies stronger mathematical constraints on the strength of the driving electric field when compared with the more general Eq. (26) and Eq. (27). Numerical tests presented in Fig. 4 (see also [32]) effectively show that the use of Eq. (29) should be avoided for modeling the nonlinear optical response in intense fields.

Funding. This research was supported by the Natural Sciences and Engineering Research Council of Canada (NSERC) through the Canada Research Chair in Ultrafast Photonics. EPOCH development was funded by the UK EPSRC grants EP/G054950/1, EP/G056803/1, EP/G055165/1 and EP/M022463/1.

Acknowledgments. The authors thank the EPOCH development and support team for their precious help. CV thanks Antonio Calà Lesina for stimulating discussions.